IEEE Access
Multidisciplinary | Rapid Review | Open Access Journal

Received August 27, 2019, accepted September 9, 2019, date of publication October 2, 2019, date of current version October 24, 2019.

Digital Object Identifier 10.1109/ACCESS.2019.2944901

Broadband Single-Layered, Single-Sided Flexible Linear-to-Circular Polarizer Using Square Loop Array for S-Band Pico-Satellites

TOUFIQ MD HOSSAIN[1,2], HIDAYATH MIRZA[1,3], PING JACK SOH[1], (Senior Member, IEEE), MOHD FAIZAL JAMLOS[4], (Senior Member, IEEE), RAIS AHMAD SHEIKH[1,3], AZREMI ABDULLAH AL-HADI[1], (Senior Member, IEEE), AND PRAYOOT AKKARAEKTHALIN[5], (Member, IEEE)

[1]Advanced Communication Engineering (ACE) CoE, School of Computer and Communication Engineering, Universiti Malaysia Perlis, Arau 02600, Malaysia
[2]School of Engineering and Information Technology, University of New South Wales, Canberra, Campbell, ACT 2600, Australia
[3]Department of Electrical Engineering, College of Engineering, Jazan University, Jazan 45142, Saudi Arabia
[4]Faculty of Mechanical Engineering, Universiti Malaysia Pahang, Pekan 26600, Malaysia
[5]Department of Electrical and Computer Engineering, Faculty of Engineering, King Mongkut's University of Technology North Bangkok (KMUTNB), Bangkok 10800, Thailand

Corresponding authors: Ping Jack Soh (pjsoh@unimap.edu.my) and Prayoot Akkaraekthalin (prayoot.a@eng.kmutnb.ac.th)

This work was supported in part by the Malaysia Ministry of Education through the Prototype Development Research Grant (PRGS) under Grant PRGS/2/2015/ICT06/UNIMAP/02/1, and in part by the Thailand Research Fund though the TRF Senior Research Scholar Program under Grant RTA 6080008.

ABSTRACT Two new flexible, single-sided linear-to-circular polarizers based on the square loop unit cells have been proposed in this work. The first uses a flexible Polydimethylsiloxane (PDMS) substrate, whereas the second polarizer is implemented on a felt textile substrate. Both polarizers uses the same ShieldIt textile to form their conducting elements. The proposed flexible single-layered structure potentially enables the implementation of the polarizer in a deployable format with improved performance consistency and reduced fabrication complexity for size- and weight-constrained applications such as in pico-satellites payloads. The textile-based design offered an improved performance and is advantageous in terms of weight compared to the PDMS-based polarizer. Besides discussing the operation principles and analyzing its surface currents, an equivalent circuit model is also proposed. Measurements of the textile-based polarizer showed satisfactory agreements with its simulated results, featuring a broad 3-dB axial ratio bandwidth of 33.57 %, operating from 1.71 GHz to 2.4 GHz. The bandwidth with at least 90 % of conversion efficiency for this structure is also improved to 47.3 % (from 1.55 GHz to 2.51 GHz), which is better than any other felt-based flexible polarizers in literature. Finally, the performance of the polarizer in different bending conditions is also assessed, indicating improved performance consistency relative to double-sided flexible polarizers.

INDEX TERMS Linear-to-circular polarizers, flexible polarizers, pico-satellites.

I. INTRODUCTION

Pico-satellites, which are cost-effective, power efficient and smaller satellites, is a viable alternative to conventional satellites [1]. These satellites are sent for diverse specialized functions including imaging, location tracking, weather monitoring, location and animal tracking etc. [2]–[5]. Cube Satellites (abbreviated as CubeSats) are one of the categories of pico-satellites usually being operated in the Low Earth Orbit (LEO), with a working lifetime of more than a few years [3], [5]. The Federal Communications Commission (FCC) has declared the S-band ranging from 2.39 GHz to 2.45 GHz as one of the recommended bands for CubeSats. Circularly-polarized (CP) waves play a vital role for the efficient operation of the satellites, maintaining communication between the satellite and the earth station, as they mitigate interference caused by multipath reflections and also in severe weather conditions such as rain fog etc. [6]. Different types of high gain antennas (HGAs) with CP characteristics have been reported for satellite applications. These include patch antennas, monopole/dipole antennas, reflector antennas, reflectarray antennas, spiral/ helical antennas etc. [1].

The associate editor coordinating the review of this manuscript and approving it for publication was Kuang Zhang.

However, designing deployable versions of these antennas with accurate CP characteristics is challenging, especially in size-restricted CubeSats (smallest size is 10 cm × 10 cm × 10 cm for 1U). Placing a linear-to-circular polarizer over a linearly polarized (LP) antenna to achieve CP waves, is considered to be a versatile solution potentially for adoption in pico-satellite communication [7], [8], [12], [19], [21]. Different linear-to-circular polarizers have been reported in the literature, starting from the multilayered meander-line-based design proposed by Young *et al.* [9] in 1973. These linear-to-circular polarizers are formed by different combinations of frequency selective structures (FSS), including multi-layered meander line structures [9], combinations of square and metallic grids [10], periodic arrangement of slotted split rings [13], and multilayered metasurface-based structures [14]–[16]. These polarizers are designed on rigid structures, which does not enable their implementation on CubeSats in deployable formats. Moreover, there is very limited work available on the design of flexible polarizers for CubeSats application.

Different multi-layered polarizers are presented in Table 1(A). It is evident that only one multi-layered polarizer has been designed in the S-band [7] from literature. The widest 3 dB axial ratio bandwidth (BW_{3dB}) of 66.7% achieved in [11] by implementing a patch array and complementary unit cell structure. However, its conversion efficiency was not assessed. Meanwhile, several other multi-layered polarizers featured BW_{3dB} of between 20 % [8] and 40 % [9]. Nonetheless, the use of multi-layered structures is very challenging in applications such as CubeSats, as the consistent spacing requirement between the multiple layers is hard to maintain when implemented using flexible materials. Therefore, the choice of single-layered polarizers is more feasible.

Next, several single-layered polarizers from literature are summarized in Table 1(B). For instance, the work in [13] presented a single layered polarizer for Terahertz (THz) applications with a BW_{3dB} of 11.75 %. Meanwhile, two metasurface-based polarizers were designed in [14] and [15] for WiFi/WiMAX applications, with the latter achieving aBW_{3dB} of 9 %. From Table 1(B) the highest BW_{3dB} of 17% was achieved by [16], which was designed using circular rings with inclined metal strip as its unit cell. The structures in Table 1(A) and (B) (regardless of the number of layers) were designed on rigid surfaces, which are unsuitable when need to be implemented in a deployable format in a CubeSat due to its stringent size constraints. Moreover, the choice of its material based on its density will also determine whether these structures will result in additional payload weight in the CubeSats. Comparison among different materials indicated that felt ([19]–[20]) featured the lowest density. Despite that, these polarizers were still designed with unit cells located on both sides of the substrate, adding complexity to the fabrication process. This is due to the need to accurately align patches on both sides of the substrate to guarantee performance consistency. Moreover, use of flexible materials and for these double-sided structures also potentially causes performance variation, especially when operated in bent conditions [19]–[21]. Among the recently designed flexible polarizers listed in Table 1(C), the highest $BW_{3\ dB}$ of 32.64 % is exhibited by [21], with the double-sided polarizer implemented on a Polydimethylsiloxane (PDMS) substrate. On the other hand, the bandwidth with at least 90% of conversion efficiency (BW_{CE}) is 6.6%, 23.88% and 48.12% from [19], [21] and [20], respectively.

In this work, a new linear-to-circular polarizer based on a single-layered and single-sided topology is designed. Compared to literature, such structure avoids the aforementioned fabrication complexities, improve its performance consistency and implementation effectiveness when intended in a deployable format due its single-sided topology and compactness (sized at $0.38\lambda_0 \times 0.36\ \lambda_0 \times 0.02\lambda_0$ per unit cell). Moreover, the proposed textile-based polarizer exhibited broader bandwidths ($BW_{3\ dB}$ and BW_{CE}) in comparison to recently reported felt-based polarizers [19], [20]. Specifically, it features a 33.57 % (from 1.71 GHz to 2.4 GHz) of $BW_{3\ dB}$ and 47.3 % (from 1.55 GHz to 2.51 GHz) of BW_{CE}.

The paper is organized as follows. Section II introduces the theory and operation of liner-to-circular polarizers, including the assessment parameters. Section III outlines the design principles of the proposed polarizer, and proposes an equivalent circuit model based on the surface current analysis. Section IV presents and analyzes the results of the polarizer both in flat and bent conditions, besides a proposed deployment process, prior to the conclusions in Section V.

II. THEORY AND OPERATION OF LINEAR-TO-CIRCULAR POLARIZERS

The electric field of a linearly polarized (LP) wave, E^i, is assumed to be incident on one side of the polarizer along positive z-axis. This E^i is aligned at an angle of 45° to the x-axis, and can be decomposed into two orthogonal field components along the x- and y axes (denoted as E_x^i and E_y^i respectively). The polarization ellipse is calculated based on the ratio of the magnitudes of the orthogonal components of the transmitted electric field along x and y axes, E_x^t and E_y^t, expressed as (1) [18], [21], [22]:

$$q = \frac{|E_x^t|}{|E_y^t|} = \frac{|E_x^i| \,.\, |T_x|}{|E_y^i| \,.\, |T_y|} \tag{1}$$

where T_x, and T_y is the transmission coefficient for E_x^i and E_y^i, respectively [6], [11], [20]. For an ideal circular polarization, the ratio in (1) should be unity, indicating an equal $|E_x^t|$ and $|E_y^t|$. The other characterizing parameter for linear-to-circular polarization is the phase difference between E_x^t and E_y^t, which ideally must be 90°, calculated as follows [17], [18]:

$$\left[\Phi_{E_x^i} + \Phi_{T_x}\right] - \left[\Phi_{E_y^i} + \Phi_{T_y}\right] = \pm n\frac{\pi}{2} \tag{2}$$

Assuming that E_x^i and E_y^i are equal in magnitude and phase, CP characteristics can be evaluated conditions (3)

TABLE 1. (a) Comparison of Recent Multi-layered Linear-to-circular Polarizers in Terms of Density, Number of Layers, Operating Band and $BW_{3\ dB}$. (b) Comparison of Recent Rigid, Single-layered Linear-to-circular Polarizers in Terms of Density, Operating Band and $BW_{3\ dB}$. (c) Comparison of Recent Flexible Single-layered Linear-to-circular Polarizers in Terms of Density, Operating Band, $BW_{3\ dB}$ and BW_{CE}.

(A)

Ref.	Substrate	Density (gm/cm^3)	Type	Application/ Operating Band	$BW_{3\ dB}$ (%)	No. of layers and sides
[6]	Rogers RT/Duroid 5880	2.2	Rigid	Ka	34.9	4
[7]	Arlon	2.31	Rigid	S-band and X-band	52	2
[8]	Rogers RT/Duroid 5880	2.2	Rigid	K	20	3
[9]	Fiber Glass	-	Rigid	X	40	4
[10]	DuPont Pyralux Polymide	-	Rigid	W	N/A	4
[11]	Arlon Diclad 880	2.31	Rigid	X	66.7	4

(B)

Ref.	Substrate	Density (gm/cm^3)	Type	Application/ Operating Band	$BW_{3\ dB}$ (%)
[12]	Rogers 5870	2.2	Rigid	K	5.6
[13]	Silicon	2.33	Rigid	THz	11.75
[14]	Rogers RO4350B	1.86	Rigid	WiFi/WiMAX	8
[15]	FR-4	1.85	Rigid	WiFi/WiMAX	9
[16]	Taconic TLX-8	2.25	Rigid	Ku	17
[17]	FR-4	1.85	Rigid	X	N/A
[18]	Rogers RT/Duroid 5870	2.2	Rigid	Ku	4.3

(C)

Ref.	Substrate	Density (gm/cm^3)	Type	Application/ Operating Band	$BW_{3\ dB}$ (%)	BW_{CE} (%)
[19]	Felt	0.25	Flexible	S	5.39	6.6
[20]	Felt	0.25	Flexible	S	N/A	48.12
[21]	PDMS	0.97	Flexible	S	32.64	23.88
This work	Felt	0.25	Flexible	S	33.57 (measured)	47.3

and (4) [18].

$$|T_x| = |T_y| \tag{3}$$

$$\Phi_{T_x} - \Phi_{T_y} = 2n\pi \pm n\frac{\pi}{2} \tag{4}$$

Besides these parameters, the CP performance can be further characterized on the basis of conversion efficiency expressed by η_{conv}. Others have defined ellipticity (η) to determine the shape of the polarization ellipse. These parameters are expressed as follows [17], [18], [20], [23]–[25]:

$$\eta_{conv} = \frac{|C_-|^2 - |C_+|^2}{|C_-|^2 + |C_+|^2} \times 100 \tag{5}$$

$$\eta = \tan^{-1}\left(\frac{|C_+| - |C_-|}{|C_+| + |C_-|}\right) \tag{6}$$

where $\boldsymbol{C}_-$ and $\boldsymbol{C}_+$ represents the circular conversion coefficient for right-handed CP wave and left handed CP wave, respectively [20].

III. POLARIZER DESIGN AND OPERATION PRINCIPLES

A. PRINCIPLE OF OPERATION AND DESIGN

From literature on metamaterials and FSSs, it can be established that the metallic components typically act as the inductive component, whereas the gaps between constituent elements of the unit cells contribute to capacitance. The value of the inductance is directly proportional to the length of the corresponding metallic element, while the capacitance depends on the spacing of the gap and its surface area. The characteristics of the transmitted wave (E^t) can be controlled by adjusting the values of inductance and capacitance interacting with one polarization to achieve the CP criteria.

These principles are considered when designing the unit cell of the proposed linear-to-circular polarizer, which is based on a square-shaped loop tilted by 45° with respect to the $x-$axis. To form the polarizer, the unit cells are connected at the $y-$direction, and are located 2 mm apart from each other in the $x-$direction. From a physical point of view, this polarizer is made to operate with broadband characteristic by first ensuring that a large transmission fractional bandwidth of the unit cell, δ, is produced by a small unit cell capacitance in the $x-$direction, C_x. This is so that $\delta = q/(\omega_0 Z_0 C_x)$; where Z_0 is the characteristic impedance of the substrate, q is the normalized quality factor of the unit cell, f_0 is the center frequency and $\omega_0 = 2\pi f_0$ [26]. On the other hand, a high inductance in the orthogonal $y-$direction is used to produce the required 90° phase compensation. The structure's continuity in the $y-$direction ensures this high inductance is produced onto the incident waves polarized in this direction. Once the level of capacitance is estimated, the phase delay in the $x-$direction can be determined. This is done by optimizing the length of the unit cell and the gap between two consecutive unit cells in the $x-$direction to result in the phase difference of 90° based on eqs. (3) and (4).

Fig. 1 shows the proposed polarizer unit cell, with its parameters specified in Table 2. The polarizer is designed on a flexible PDMS and felt substrate with a relative permittivity

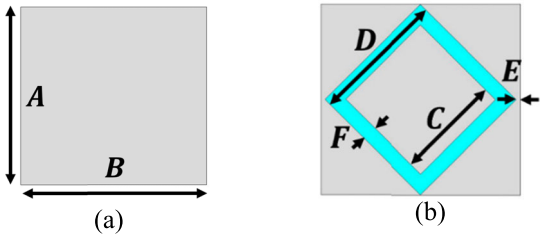

FIGURE 1. The proposed square-shaped polarizer unit cell (a) front view (b) back view.

TABLE 2. Dimensions (in mm) of the proposed designs.

Parameter	Value (mm)	
	PDMS-based design	Textile-based design
A	38.5	46
B	40.5	48
C	20.1	25.5
D	27.2	32.5
E	1	1
F	3.5	3.5

(ε_r) of 2.7 and 1.44, respectively. Meanwhile, the square loop is formed using ShieldIt conductive textile, with an electric conductivity of 1.18 x 10^5 S/m. CST Microwave Studio was used to design and optimize the dimension of structure.

Note that this polarizer is single sided in contrast to the previous double-sided polarizers designed in [19], [20]. The advantage of the single sided design includes the simplicity in fabrication and reduced complexity of alignment on both sides for the polarizer for optimized performance.

B. EQUIVALENT CIRCUIT MODEL

To simplify future design procedure of the polarizer, an equivalent circuit model is modelled. The circuit model is modeled based on the $x-$ and $y-$polarized incident waves presented in Fig. 2. It can be seen that in the $x-$ polarization, the inductance (L_x) is 8.4 nH, which is lower the value of 14.9 nH in the y-directed polarization (L_y). As aforementioned, the lower values of inductance can be attributed to the length discontinuities of the conductive elements in the unit cells in the $x-$direction.

On the other contrary, the connections between unit cells in the $y-$ direction resulted in the higher value of inductance, as also explained in Section II (A). Similarly, in the equivalent circuit model, the $x-$polarized capacitance (C_x) indicated a value of 0.2 pF, whereas a higher $y-$polarized capacitance (C_y) of 7 pF is produced. The higher capacitance in the $y-$ direction is due to the smaller gap area in proximity of the junction. On the other hand, the unit cells are 2 mm apart from each other in $x-$direction, which then reduces its capacitance to 0.2 pF. A comparison between the simulated transmission characteristics from the modeled circuit and the full wave EM simulation is presented in Fig. 2(c), indicating good agreements in terms of transmission characteristics.

The transmission characteristics of the $x-$ polarized waves is initially higher at lower frequencies and gradually decreases in value as frequency increases, with a -10 dB value at 3 GHz. On the other hand, the $y-$ polarized transmission coefficient shows the opposite characteristics.

To obtain further insights of the operating principles of the polarizer, the surface current analysis of the unit cell in the x- and $y-$ polarization are illustrated in Fig. 3. It is evident from Fig. 3(a) that the existence of the relatively large spacing of 2 mm in the $x-$ direction resulted in minimum surface currents at this direction. Relatively stronger surface currents are more concentrated on the inner sections of the top and bottom corners of the unit cells, and this level gradually degraded towards the outer perimeters of the loop structure. Meanwhile, the continuity of the unit cell structure in the $y-$direction resulted in a more dense surface current in this direction compared to the $x-$directed polarization. Moreover, it can be observed that the smaller gap at the junction of the two unit cells in the $y-$direction resulted in the concentration of higher surface currents on the outer sections at the top and bottom corners of the unit cells, as seen in Fig. 3(b). The strength of the surface currents degraded towards the inner perimeters of the square loop, contrary to the previous observation for the transmission of the $x-$directed polarized waves.

C. FABRICATION OF THE POLARIZER AND MEASUREMENT SETUP

As aforementioned, that the textile based design has been chosen for fabrication and further investigation assessment due to its better performance. The fabrication the conductive textile is performed using laser printing (dimensioned using a flat-bed fiber laser cutting machine (Glorystar GS-3015)) shown in Fig. 4(a), whereas the measurement setup is presented in Fig 4(b).

The important steps in fabricating the polarizer can be summarized as follows:

- The final optimized design is exported into a Gerber file format from the electromagnetic simulator.
- The exported Gerber file is then imported into the flat-bed fiber laser cutting machine (model Glorystar GS-3015) as shown in Fig. 4(a).
- Shieldit Super^{TM} conductive textile from LessEMF Inc is inserted and dimensioned using the laser cutting machine.
- Completed samples of unit cells are checked for dimensional accuracies. If not satisfactory, re-fabrication will take place.
- Dimensioned unit cells are then secured onto the felt substrate carefully using ironing. This can be performed easily as ShieldIt features a hot-melt adhesive on its reverse side.
- Distance between adjacent unit cells are checked to ensure accuracy. If not satisfactory, re-fabrication will take place.

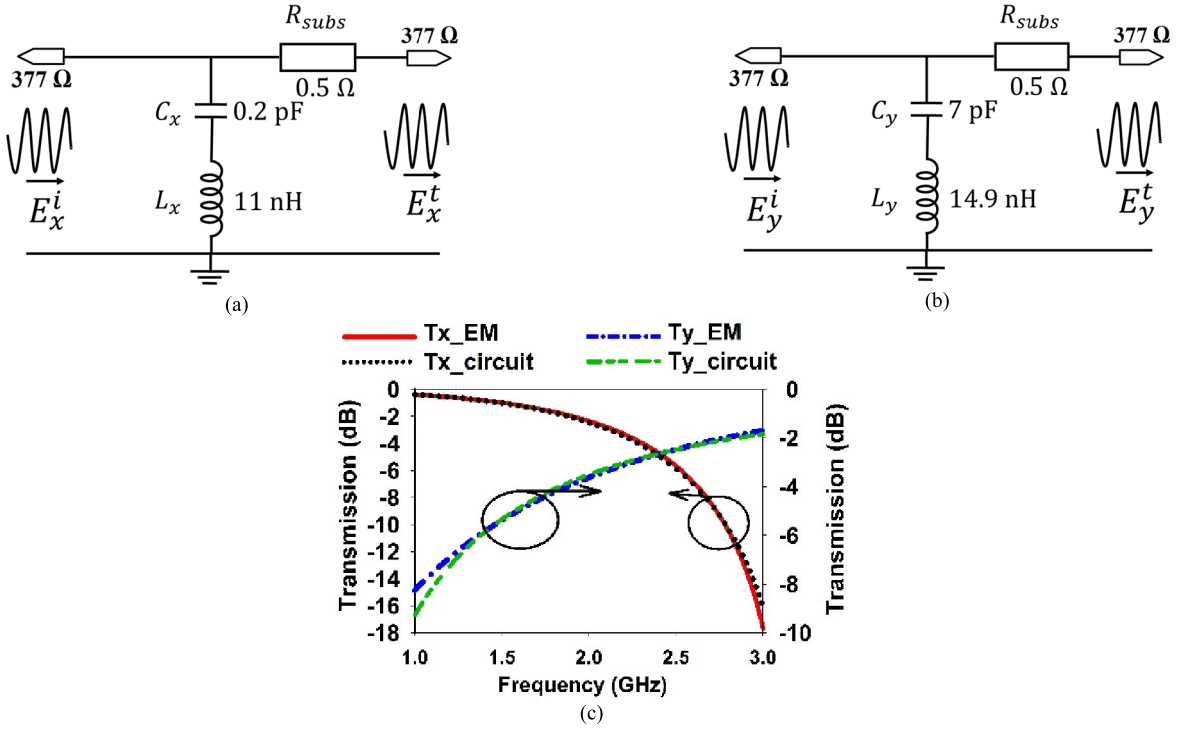

FIGURE 2. Equivalent circuit model for (a) $x-$polarization and, (b) $y-$polarization, (c) comparison between circuit and EM simulations.

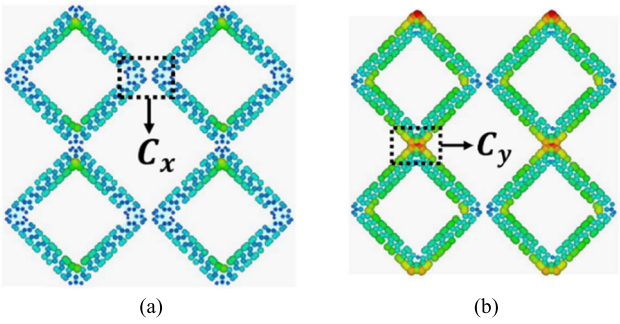

FIGURE 3. Surface current J_{surf} of the proposed polarizer at the (a) $x-$polarization (b) $y-$polarization.

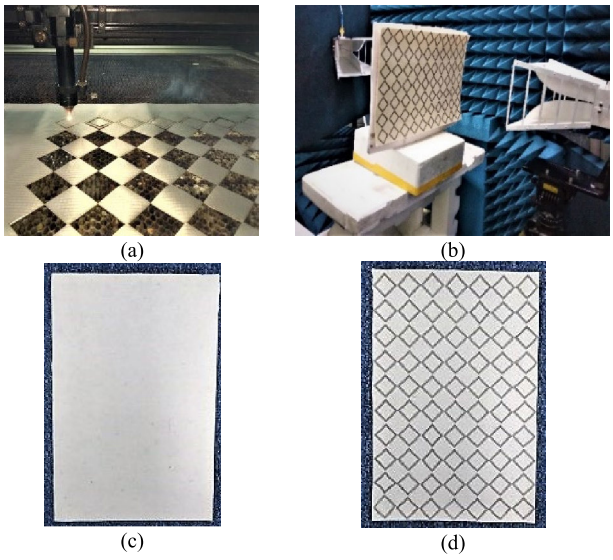

FIGURE 4. (a) Laser cutting process during the fabrication of Shieldit textile, (b) measurement setup, (c) fabricated prototype (front view), and (d) fabricated prototype (back view).

Next, the completed polarizer is experimentally assessed based on the method described in [27]–[29]. It is placed between a pair of transmitting and receiving horn antennas (A-INFOMW LB-8180-NF (0.8-18 GHz)) in the far field region, as depicted in Fig. 4(b).

IV. PERFORMANCE ASSESSMENT OF POLARIZERS

A. DEPLOYED CONDITION

In this work, two designs, one PDMS-based and the other textile-based are compared. In both cases, ShieldIt Super^{TM} conductive textile from LessEMF Inc is used to build the square loop unit cells for both substrates. The transmission characteristics of both polarizers are shown in Fig. 5, indicating similarity at the x- and $y-$ polarization. For the transmission coefficient in the $x-$ polarization, $T_x$has equal value to that of the $y-$ polarized T_y at 2.22 GHz for the case of PDMS-based design. This intersection is also observed at 2.18 GHz for the textile-based design (in simulations) and at 2.14 GHz (in measurements). Besides that, the phase difference between the x- and $y-$polarized transmission coefficient

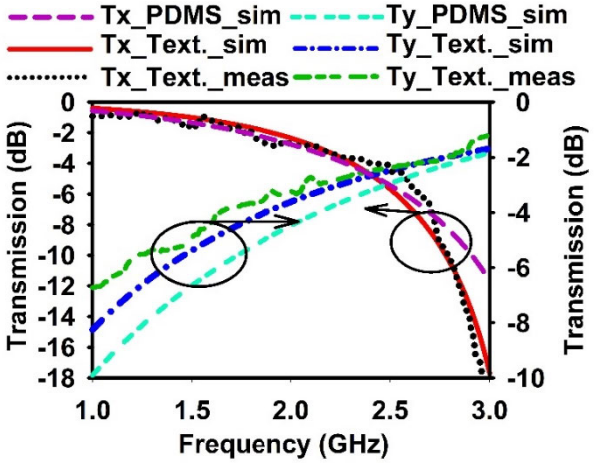

FIGURE 5. Transmission coefficient of the *x* and *y* polarized components for the PDMS- and textile-based designs in flat condition.

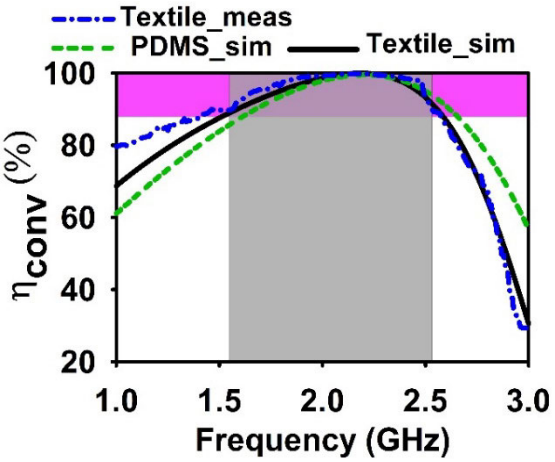

FIGURE 7. Conversion efficiency (η_{conv}) of the proposed polarizer in flat condition.

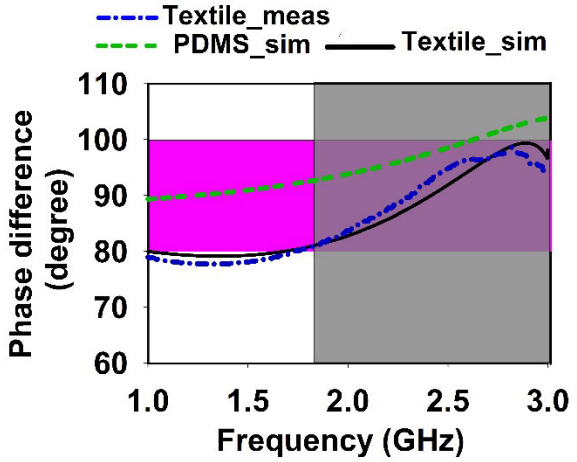

FIGURE 6. Phase difference between T_y and T_x ($\Phi_{Ty} - \Phi_{Tx}$) in flat condition.

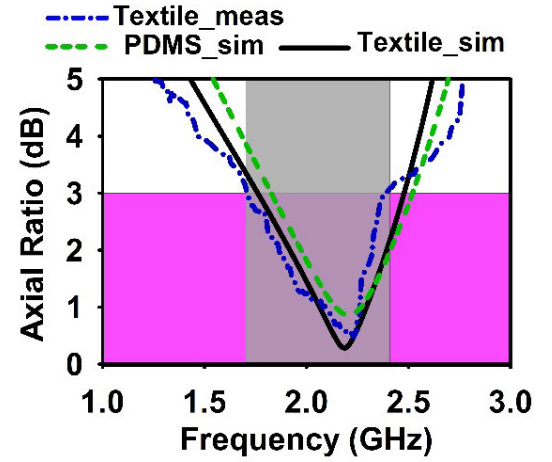

FIGURE 8. Axial ratio (AR) of the proposed polarizer in flat condition.

presented in Fig. 6 indicated that the phase criteria in (4) is fulfilled by the polarizer over the S- band.

In broadband designs, a tolerance of $\pm\mathbf{10}^\circ$ in the phase difference is typically considered. This effectively renders the operation of the polarizer from 1 GHz to 2.62 GHz (for the PDMS-based design) and from 1.67 GHz to 3 GHz (in simulations) and from 1.74 GHz to 3 GHz (in measurements) for the textile-based design. In Fig. 6, the purple-shaded zone represents the area with a phase difference of $\mathbf{90}^\circ \pm \mathbf{10}^\circ$, whereas the silver-shaded zone represents the frequency band with such phase difference. This indicated the fulfillment of the phase characteristics in the S-band.

The conversion efficiency ($\eta_{\mathbf{conv}}$), axial ratio (AR) and ellipticity (η) of the proposed polarizer is presented in Fig. 7, Fig. 8 and Fig. 9 respectively. In these figures, the purple-shaded zones represent the target parameter ranges of the polarizer: $\eta_{\mathbf{conv}} > 90$ % (in Fig. 7), AR < 3 dB (in Fig. 8) and $40^\circ > \eta > 45^\circ$ (in Fig. 9). On the other hand, the silver-shaded zone represents the achieved characteristics of these parameters and their frequency bands. The PDMS-based polarizer has shown a conversion efficiency higher than 90% from 1.68 GHz to 2.62 GHz in simulations (see Fig. 7) which corresponds to bandwidth $\boldsymbol{BW_{CE}}$ of 43.73 %. On the other hand, the textile-based polarizer has outperformed the PDMS-based polarizer with a bandwidth BW_{CE} of 47.7 % (from 1.58 GHz to 2.57 GHz) in simulations and 47.3 % (from 1.55 GHz to 2.51 GHz) in measurements. Note that the values in Fig. 7 are not representative of the material losses, as the η_{conv} parameter are calculated based on the squared magnitude of the circular polarization conversion coefficients (C_+ and C_-) based on eq. (5). These values, both in simulations or measurements results in relative values, which is then converted into percentage.

In the case of the 3dB AR bandwidth, $BW_{3\ dB}$ is 32.3 % (from 1.82 GHz to 2.52 GHz) for PDMS-based design. Meanwhile, the textile-based design featured wider $BW_{3\ dB}$ relative to the PDMS-based design with 34.73 % (from 1.76 GHz to 2.5 GHz) in simulations and 33.57 % (from 1.71 GHz to 2.4 GHz) in measurements. Finally, the ellipticity of the polarizer (in degrees) is shown in Fig. 9(a). Fig. 9(b) shows the polarization azimuth characteristics whereas Fig. 9(c) shows polarization ellipses at different frequencies. Measurements indicated an ellipticity of between 40° and 45° from 2 GHz to 2.4 GHz (18.18 %). On the other hand, for

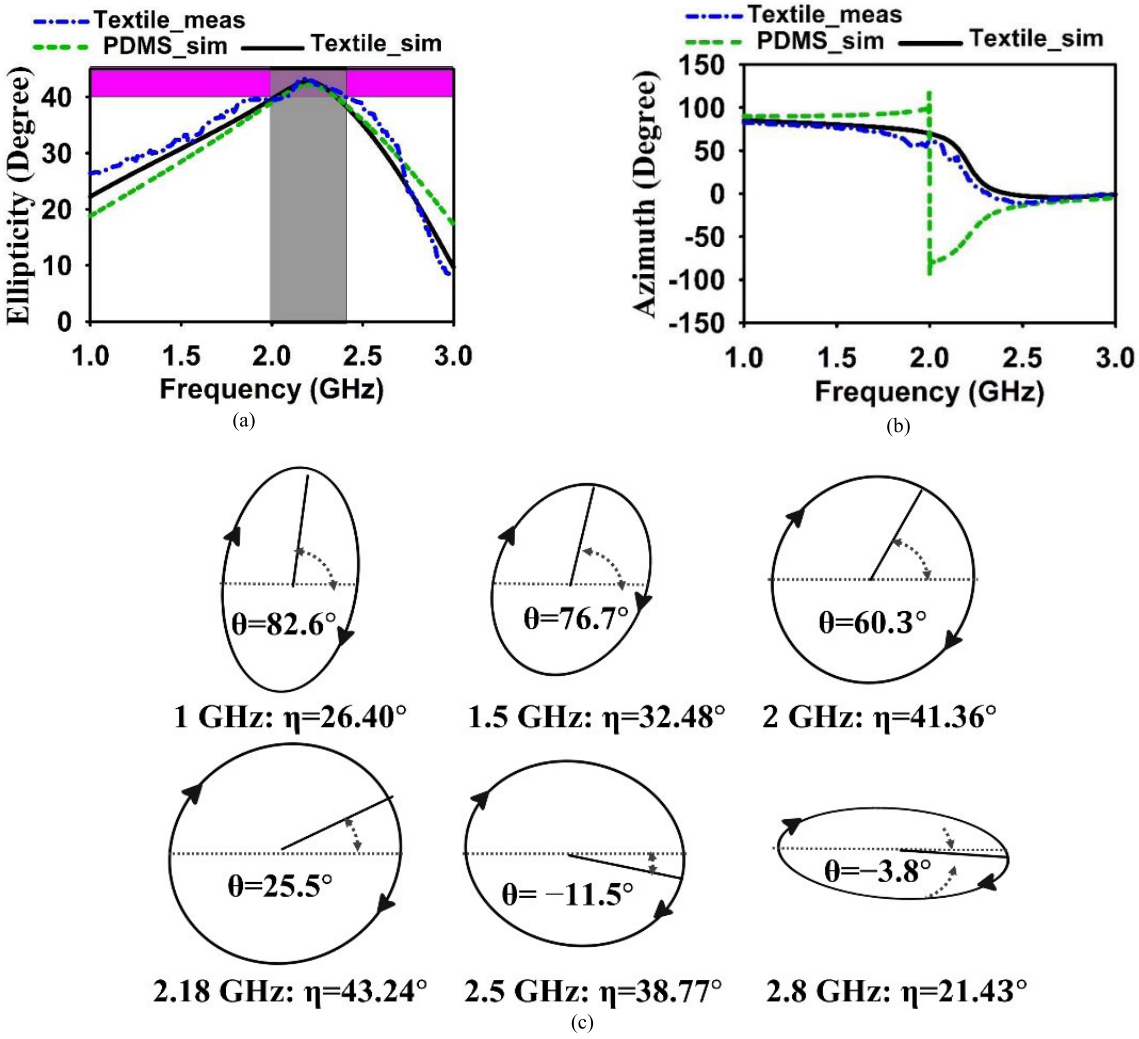

FIGURE 9. Depiction of (a) ellipticity, (b) azimuth and (c) measured polarization ellipses at different frequencies in flat condition.

the PDMS-based design, this zone is observed to be from 2.05 GHz till 2.35 GHz (13.63 %) in simulations.

In comparison, this band is observed to be from 2.02 GHz to 2.36 GHz (15.53 %) in the case the textile-based design in simulations. It is found that the measured results agreed very well with the simulations of the textile-based design.

From Fig. 9(c), it can be seen that the polarizer featured a left handed polarization (considering wave propagation outwards from the viewing plane). Moreover, the main polarization axis is rotated towards the clockwise direction with the increase in frequency, as can be seen from the azimuth angles depicted by $\theta = 82.6°, 76.7°, \ldots, 38.77°$. Furthermore, between 2 GHz and 2.4 GHz, the shape of the ellipse is quasi-circular due to the ellipticity value of between 40° and 45°. For example, the ellipticity is 41.36° at 2 GHz, whereas at 2.18 GHz it is 43.24°. This polarization ellipse is more elliptical in shape from 2.4 GHz onwards, as the ellipticity is reduced from 40° and less, as shown in Fig. 9. The detailed performance of the polarizer is presented in Table 3.

To ensure a fair comparison, the final operating bandwidth of the polarizer is determined based on the fulfillment of all four operational requirements: (a) the conversion efficiency, η_{conv} better than 90%, (b) phase difference of 90° with a tolerance of +10° or −10°, (c) ellipticity, η varying from 40° to 45°, and (d) axial ratio, AR less than 3 dB. It can be seen from Table 3 that the proposed textile-based polarizer featured improvement in performance compared to the PDMS-based version, with an operational bandwidth of 15.53 % in simulations and 14.77 % in measurements. At its optimal point (the intersection of the T_x and T_y), the textile-based polarizer has shown a conversion efficiency, ellipticity and AR of 99.82 %, 43.27°, and 0.53 dB respectively. Meanwhile, whereas the PDMS-based polarizer has shown values of 99.5%, 42.13°, 0.87 dB, respectively at the same optimal operating point.

B. ASSESSMENT IN BENT CONDITION AND DEPLOYMENT PROCESS

To analyze the possible changes in performance due to the use of flexible substrate, the textile-based polarizer is assessed when bent over a vacuum cylinder of 100 mm in radius in four different bending conditions. In each of $x-$ and $y-$axis, the bending has been performed in two scenarios, inwards and

TABLE 3. Summary of the performance of proposed polarizers when assessed in a flat (deployed) condition.

Design	Substrate	Frequency band (GHz)					$\lvert T_x\rvert = \lvert T_y\rvert$				
		η_{conv} > 90 %	Ellipticity $40^\circ < \eta < 45^\circ$	Phase Diff. ($90^\circ \pm 10^\circ$)	AR<3 dB	Operational bandwidth	Freq. (GHz)	$\Delta\Phi$ ($^\circ$)	η_{conv}	η ($^\circ$)	AR
PDMS (Design 1)	Simulated	1.68-2.62	2.05-2.35	1-2.62	1.82-2.52	2.05-2.35 (13.63 %)	2.22	95.74	99.5%	42.13	0.87
Textile (Design 2)	Simulated	1.58-2.57	2.02-2.36	1.67-3	1.76-2.5	2.02-2.36 (15.53 %)	2.18	85.33	99.67%	42.67	0.7
	Measured	1.55-2.51	2.07-2.4	1.74-3	1.71-2.4	2.07-2.4 (14.77 %)	2.14	86.62	99.82%	43.27	0.53

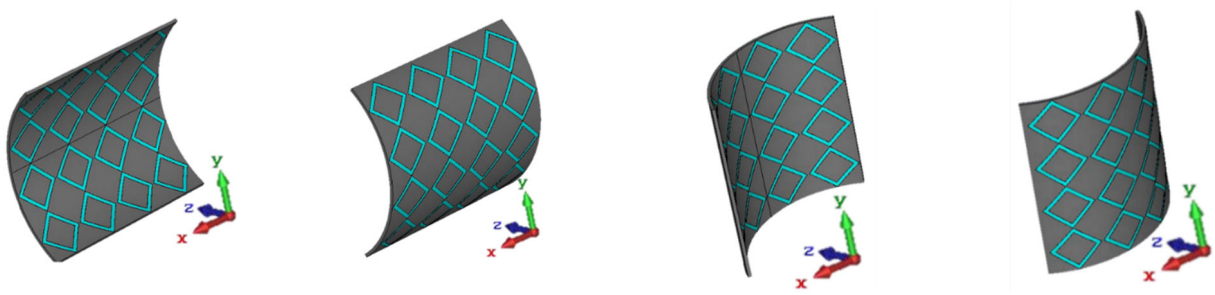

(a) (b) (c) (d)

FIGURE 10. Illustration of different bending geometry: $x-$axis bending (a) inward, (b) outward; $y-$axis bending (c) inward, (d) outward.

outwards, as shown in Fig. 10. Generally, the two additional types of bending is each denoted as $x-$ or $y-$axis bending, depending on the alignment of the vacuum cylinder towards these axes. For the case of inwards bending, the proposed polarizer is bent around the vacuum cylinder when it is placed on the reverse side of the polarizer. Conversely, outwards bending is realized when the vacuum cylinder is placed on the front face of the polarizer.

Figs. 11, 12 and 13 present the performance of the polarizer in terms of AR, conversion efficiency (η_{conv}), and ellipticity (η). In general, the variation of these parameters can be attributed to the changes in capacitance and inductance in line with the physical modifications in spacing and coupling when bent. This then results in the deviation of the transmitted waves from the desired CP characteristics. From the results, it is observed that the two $x-$axis bending conditions (inwards and outwards) performed better in comparison to when the polarizer is bent at the $y-$axis. Specifically for the $x-$axis bending, the polarizer starts to operate with an under 3dB AR at 1.78 GHz, as illustrated in Fig. 11. This indicated a BW_{3dB} of 31.3 % and operation from 1.78 GHz to 2.44 GHz when bent inwards. Meanwhile when bent outwards, the operating bands with at least 3dB of AR is seen to be separated into two bands, from 1.7 GHz to 2.07 GHz and from 2.456 GHz to 2.46 GHz corresponding to BW_{3dB}

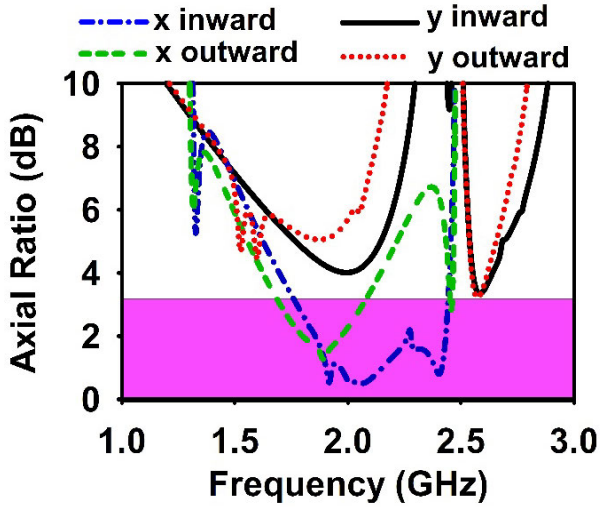

FIGURE 11. Axial ratio (AR) with different bending conditions.

of 19.63 % and 0.16 %. On the contrary, when the polarizer is bent at the $y-$axis in both inwards and outwards conditions, the 3 dB AR criteria is not met despite its AR improvement when approaching 1.9 GHz.This observation also serves as an indication of the better expected performance of the polarizer when bent at the $x-$axis compared to bending at the $y-$axis in terms of conversion efficiency and ellipticity.

TABLE 4. Performance summary of proposed polarizers when assessed in different bending conditions.

Performance assessing property	Frequency bands (GHz))			
	x −axis bending		y −axis bending	
	Inwards	Outwards	Inwards	Outwards
Axial ratio, AR<3 dB	1.78-2.44 (31.3%)	1.7-2.07 and 2.456-2.46 (19.63% and 0.16%)	NA	NA
Conversion efficiency, η_{conv} >90%	1.69-2.45 (36.71%)	1.62-2.15 and 2.45-2.46 (28.12% and 0.4%)	1.96-2.03 and 2.55-2.64 (3.5% and 3.47%)	2.55-2.62 (2.7%)
Ellipticity, η=40˚-45˚	1.88- 2.22 and 2.34-2.43 (16.59% and 0.38%)	1.88-1.912 (1.68%)	NA	NA

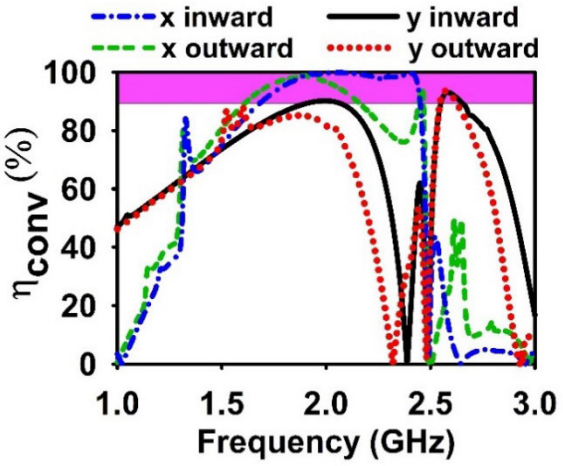

FIGURE 12. Conversion efficiency (η_{conv}) of the polarizer under different bending conditions.

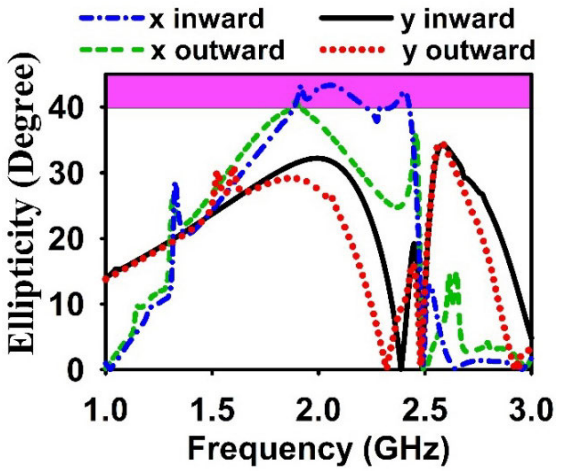

FIGURE 13. Ellipticity (η) of the polarizer under different bending conditions.

From Fig. 12, both cases of x−axis bending resulted in an improving conversion efficiency for the polarizer. It started operating with 90 % of η_{conv} at 1.6 GHz. However, the η_{conv} when the polarizer is bent outwards (denoted by green dotted graph) did not follow the same trend as the $\eta_{conv}$of the polarizer bent inwards (denoted by blue dotted graph). The BW_{CE} is 36.71 % (from 1.69 GHz to 2.45 GHz) when the polarizer is bent at the x−axis inwards, whereas two BW_{CE} of 28.12 % (from 1.62 GHz to 2.15 GHz) and 0.4 % (from 2.45 GHz to 2.46 GHz) are observed when bent outwards.

Meanwhile, for η_{conv} in the y−axis, two main bands are observed to achieve a value of at least 90 % when bent inwards: i) from 1.96 GHz to 2.03 GHz (3.5 %); and ii) from 2.55 GHz to 2.64 (3.47%). On the other hand, a small operating band is observed in the case of outward y− axis bending, i.e. from 2.55 GHz to 2.62 GHz, with a BW_{CE} of 2.71 %. In Fig. 13, it is seen that both inwards and outwards bending configurations of the polarizer at the x−axis similarly improved ellipticity (η) to an acceptable level at approximately 1.9 GHz. However, similar to the case of conversion efficiency, the outward bending of the polarizer (green dotted graph) did not perform as well as the inward bending (blue dotted graph) in terms of ellipticity. Therefore, the bandwidth with ellipticity of at least 40° is 16.59 % (from 1.88 GHz to 2.22 GHz) and 0.38 % (from 2.34 GHz to 2.43 GHz) when bent inwards at the x−axis, while only 1.68 % of ellipticity (from 1.88 GHz to 1.912 GHz) is produced when the polarizer is bent outwards at the x−axis.

Despite being acceptable in terms of conversion efficiency, bending of the polarizer at the y−axis, however, is unfavorable in terms of ellipticity and AR. This is attributed to the change of capacitance (C_y), due to change of shape in the connecting junction of the polarizer unit cells when bent at the y-axis (see Fig. 3).To conclude, while the deployment process should ensure the flat operation of the polarizer, any fail-safe deployable mechanism must allow the bending inwards at the x−axis for better operation.

V. CONCLUSION

A single sided linear-to-circular polarizer designed on flexible textile material has been proposed for S-band CubeSats application. The polarizer is designed using an array of square-shaped loop unit cells. Two different flexible material have been used as its substrate: PDMS and felt textile. A detailed description of its design principles and the proposal of an equivalent circuit model and surface current analysis is first presented. The performance of both polarizers are then assessed in terms of phase difference, axial ratio, conversion efficiency, ellipticity and polarization azimuth. The textile-based design was chosen for fabrication and further evaluation due to its better performance indicated in simulations. It is observed to operate from 1.74 GHz to 3 GHz

with a phase difference between T_x and T_y of $90°\pm10°$. The polarizer indicated a 3 dB axial ratio bandwidth of 33.57 % (from 1.71 GHz to 2.4 GHz), whereas the bandwidth with at least 90 % of conversion efficiency is 47.3 % (from 1.55 GHz to 2.51 GHz). Meanwhile, its bandwidth fulfilling the ellipticity of between 40° and 45° is observed to be from 2 GHz to 2.4 GHz (18.18 %). To ensure that the deployable polarizer can be used in a fail-safe condition on CubeSats, the polarizer is assessed further under different bending conditions. It is observed that the most favorable fail-safe deployment process should allow the polarizer to be bent inwards at the $x-$axis compared to the other bending conditions, when studied in terms of axial ratio, conversion efficiency and ellipticity. Finally, it can be concluded that the performance exhibited by the proposed polarizer when assessed under different conditions meets the requirements for future integration in S-band CubeSats.

REFERENCES

[1] A. H. Lokman, P. J. Soh, S. N. Azemi, H. Lago, S. K. Podilchak, S. Chalermwisutkul, M. F. Jamlos, A. Abdullah Al-Hadi, P. Akkaraekthalin, and S. Gao, "A review of antennas for picosatellite applications," *Int. J. Antennas Propag.*, vol. 2017, Apr. 2017, Art. no. 4940656. doi: 10.1155/2017/4940656.

[2] R. E. Hodges, D. J. Hoppe, M. J. Radway, and N. E. Chahat, "Novel deployable reflectarray antennas for CubeSat communications," in *IEEE MTT-S Int. Microw. Symp. Dig.*, May 2015, pp. 4–7.

[3] C. J. Vourch and T. D. Drysdale, "Inter-CubeSat communication with V-band 'Bull's eye' antenna," in *Proc. 8th Eur. Conf. Antennas Propag. (EuCAP)*, Apr. 2014, pp. 3545–3549.

[4] N. Chahat, R. Hodges, J. Sauder, M. Thomson, and Y. Rahmat-Samii, "Earth science RADAR CubeSat deployable Ka-band mesh reflector antenna," in *Proc. IEEE Int. Symp. Antennas Propag. (APSURSI)*, Jun. 2016, pp. 1531–1532.

[5] N. Chahat, R. E. Hodges, J. Sauder, M. Thomson, and Y. Rahmat-Samii, "The Deep-Space Network Telecommunication CubeSat Antenna: Using the deployable Ka-band mesh reflector antenna," *IEEE Antennas Propag. Mag.*, vol. 59, no. 2, pp. 31–38, Apr. 2017.

[6] L. Martinez-Lopez, J. Rodriguez-Cuevas, J. I. Martinez-Lopez, and A. E. Martynyuk, "A multilayer circular polarizer based on bisected split-ring frequency selective surfaces," *IEEE Antennas Wireless Propag. Lett.*, vol. 13, pp. 153–156, 2014.

[7] M. Fartookzadeh and S. H. M. Armaki, "Dual-band reflection-type circular polarizers based on anisotropic impedance surfaces," *IEEE Trans. Antennas Propag.*, vol. 64, no. 2, pp. 826–830, Feb. 2016.

[8] M. Hosseini and S. V. Hum, "A circuit-driven design methodology for a circular polarizer based on modified Jerusalem cross grids," *IEEE Trans. Antennas Propag.*, vol. 65, no. 10, pp. 5322–5331, Oct. 2017.

[9] L. Young, L. A. Robinson, and C. Hacking, "Meander-line polarizer," *IEEE Trans. Antennas Propag.*, vol. AP-21, no. 3, pp. 376–378, May 1973.

[10] C. Dietlein, A. Luukanen, Z. Popović, and E. Grossman, "A W-band polarization converter and isolator," *IEEE Trans. Antennas Propag.*, vol. 55, no. 6, pp. 1804–1809, Jun. 2007.

[11] W. Zhang, J.-Y. Li, and L. Wang, "Broadband circular polarizer based on multilayer gradual frequency selective surfaces," *Int. J. Antennas Propag.*, vol. 2016, Aug. 2016, Art. no. 4928109. doi: 10.1155/2016/4928109.

[12] Y. Ranga, L. Matekovits, S. G. Hay, and T. S. Bird, "An anisotropic impedance surface for dual-band linear-to-circular transmission polarization convertor," in *Proc. Int. Workshop Antenna Technol. (iWAT)*, Mar. 2013, pp. 47–50.

[13] M. Eular, V. Fusco, R. Cahill, and R. Dickie, "325 GHz single layer submillimeter wave FSS based split slot ring linear to circular polarization convertor," *IEEE Trans. Antennas Propag.*, vol. 58, no. 7, pp. 2457–2459, Jul. 2010.

[14] H. L. Zhu, S. W. Cheung, K. L. Chung, and T. I. Yuk, "Linear-to-circular polarization conversion using metasurface," *IEEE Trans. Antennas Propag.*, vol. 61, no. 9, pp. 4615–4623, Sep. 2013.

[15] H. Zhu, K. L. Chung, X. L. Sun, S. W. Cheung, and T. I. Yuk, "CP metasurfaced antennas excited by LP sources," in *Proc. IEEE Int. Symp. Antennas Propag.*, Jul. 2012, pp. 1–2.

[16] X. Ma, C. Huang, M. Pu, C. Hu, Q. Feng, and X. Luo, "Single-layer circular polarizer using metamaterial and its application in antenna," *Microw. Opt. Technol. Lett.*, vol. 54, no. 7, pp. 1770–1774, Jul. 2012.

[17] S. Yan and G. A. E. Vandenbosch, "Compact circular polarizer based on chiral twisted double split-ring resonator," *Appl. Phys. Lett.*, vol. 102, no. 10, Mar. 2013, Art. no. 103503.

[18] I. Sohail, Y. Ranga, K. P. Esselle, and S. G. Hay, "A linear to circular polarization converter based on Jerusalem-Cross frequency selective surface," in *Proc. 7th Eur. Conf. Antennas Propag.*, Apr. 2013, pp. 2141–2143.

[19] H. Mirza, T. M. Hossain, P. J. Soh, M. F. Jamlos, M. N. Ramli, E. S. Hassan, A. A. Al-Hadi, and S. Yan, "Single layered swastika-shaped flexible linear-to-circular polarizer using textiles for S-band application," *Int. J. RF Microw. Comput.-Aided Eng.*, vol. 28, no. 7, Sep. 2018, Art. no. e21463.

[20] H. Mirza, P. J. Soh, M. F. Jamlos, T. M. Hossain, M. N. Ramli, A. A. Al-Hadi, R. A. Sheikh, E. S. Hassan, and S. Yan, "A crossed dodecagonal deployable polarizer on textile and polydimethylsiloxane (PDMS) substrates," *Appl. Phys. A, Solids Surf.*, vol. 124, p. 178, Feb. 2018.

[21] H. Mirza, T. M. Hossain, P. J. Soh, M. F. Jamlos, M. N. Ramli, A. A. Al-Hadi, E. S. Hassan, S. Yan, "Deployable linear-to-circular polarizer using PDMS based on unloaded and loaded circular FSS arrays for Pico-satellites," *IEEE Access*, vol. 7, pp. 2034–2041, 2018.

[22] Y. Ranga, D. Thalakotuna, K. P. Esselle, S. G. Hay, L. Matekovits, and M. Orefice, "A transmission polarizer based on width-modulated lines and slots," in *Proc. Int. Workshop Antenna Technol. (iWAT)*, Mar. 2013, pp. 299–302.

[23] M. Mutlu, A. E. Akosman, and E. Ozbay, "Broadband circular polarizer based on high-contrast gratings," *Opt. Lett.*, vol. 37, no. 11, pp. 2094–2096, 2012.

[24] H.-X. Xu, G.-M. Wang, M. Q. Qi, T. Cai, and T. J. Cui, "Compact dual-band circular polarizer using twisted Hilbert-shaped chiral metamaterial," *Opt. Express*, vol. 21, no. 21, pp. 24912–24921, 2013.

[25] J. Wang, Z. Shen, W. Wu, and K. Feng, "Wideband circular polarizer based on dielectric gratings with periodic parallel strips," *Opt. Express*, vol. 23, no. 10, pp. 12533–12543, 2015.

[26] N. Behdad and M. A. Al-Joumayly, "A generalized synthesis procedure for low-profile, frequency selective surfaces with odd-order bandpass responses," *IEEE Trans. Antennas Propag.*, vol. 58, no. 7, pp. 2460–2464, Jul. 2010.

[27] J. D. Baena, S. B. Glybovski, J. P. del Risco, A. P. Slobozhanyuk, and P. A. Belov, "Broadband and thin linear-to-circular polarizers based on self-complementary zigzag metasurfaces," *IEEE Trans. Antennas Propag.*, vol. 65, no. 8, pp. 4124–4133, Aug. 2017.

[28] P. Fei, Z. Shen, X. Wen, and F. Nian, "A single-layer circular polarizer based on hybrid meander line and loop configuration," *IEEE Trans. Antennas Propag.*, vol. 65, no. 10, pp. 4609–4614, Oct. 2015.

[29] L. Wu, Z. Yang, Y. Cheng, R. Gong, M. Zhao, Y. Zheng, J. Duan, and X. Yuan, "Circular polarization converters based on bi-layered asymmetrical split ring metamaterials," *Appl. Phys. A, Solids Surf.*, vol. 116, no. 2, pp. 643–648, Feb. 2014.

TOUFIQ MD HOSSAIN was born in Al-Kharj, Saudi Arabia, in 1991. He received the B.Sc. degree in electrical and electronic engineering (EEE) from the Khulna University of Engineering & Technology (KUET), Khulna, in 2014, the M.Sc. degree in communication engineering from Universiti Malaysia Perlis (UniMAP), in 2018, where he was a Research Assistant, until April 2019. He is currently pursuing the Ph.D. degree with the School of Engineering and Information Technology, University of New South Wales (UNSW), Canberra, sponsored by the TFS Scholarship from UNSW. He has authored or coauthored eight refereed journals and nine international conference papers. His research interests include metamaterial imaging, flexible linear to circular polarizers, microwave reflectometers, and microwave imaging of brain injury diagnosis applications.

HIDAYATH MIRZA was born in Hyderabad, India, in 1981. He received the bachelor's degree in electronics and communication engineering from Jawaharlal Nehru Technological University (JNTU), Hyderabad, India, in 2005, and the M.S. degree in radio engineering from Kyung Hee University (KHU), South Korea, in 2008. He is currently pursuing the Ph.D. degree with the School of Computer and Communication Engineering, Universiti Malaysia Perlis (UniMAP), Malaysia. From 2006 to 2008, he was a Research Assistant with the Wireless Technology Laboratory, Kyung Hee University, and from 2009 to 2011, he was a full time Researcher with the ESAT-TELEMIC Research Division, KU Leuven, Belgium. Since 2012, he has been a Lecturer at the Department of Electrical Engineering, Jazan University, Jazan, Saudi Arabia. His research interests include wearable antennas, RF energy scavenging using rectenna, RFID tag antenna design, characterization of materials, extraction of permittivity, metamaterials, and flexible linear-to-circular polarizers. He was a recipient of the Young Scientist Travel Grant (YSTG), the 2007 International Symposium on Antennas and Propagation (ISAP), and the KHU President's Scholarship for four consecutive semesters, from 2006 to 2008.

PING JACK SOH (S'10–M'14–SM'15) was born in Sabah, Malaysia. He received the B.Eng. and M.Eng. degrees from Universiti Teknologi Malaysia and the Ph.D. degree from KU Leuven, Belgium.

From 2002 to 2004, he was a Test Engineer with Venture Corporation. In 2005, he joined Motorola Solutions Malaysia, as a Research and Development Engineer. In 2006, he was a Lecturer with Universiti Malaysia Perlis (UniMAP). From 2009 to 2013, he was a Research Assistant with the ESAT-TELEMIC Research Division, KU Leuven, before pursuing his Ph.D. degree, where he was a Postdoctoral Fellow, from 2013 to 2014. He is currently an Associate Professor with the School of Computer and Communication Engineering, Universiti Malaysia Perlis (UniMAP), and a Research Affiliate at KU Leuven. He researches actively in the areas of interests: wearable and flexible antennas/metasurfaces, on-body communication, electromagnetic safety and absorption, and wireless and radar techniques for healthcare applications.

Dr. Soh is a member of the IET and URSI. He was a recipient of the IEEE AP-S Doctoral Research Award, in 2012, the IEEE MTT-S Graduate Fellowship for Medical Applications, in 2013, and the URSI Young Scientist Award, in 2015. He was also the second place winner of the IEEE Presidents' Change the World Competition in 2013. He is a Chartered Engineer registered with the U.K. Engineering Council and a Professional Technologist registered with the Malaysia Board of Technologist (MBOT). He also serves in the IEEE MTT-S Education Committee and the IEEE MTT-S Meetings and Symposia (M&S) Committee.

MOHD FAIZAL JAMLOS received the B.Eng degree (Hons.) in computer engineering from Universiti Malaysia Perlis, Malaysia, in 2006, the M.Sc. degree from The University of Adelaide, SA, Australia, in 2008 and the Ph.D. degree from Universiti Teknologi Malaysia, Johor, Malaysia, in 2010. He is currently a Full Professor with the Faculty of Mechanical Engineering, Universiti Malaysia Pahang. He has coauthored more than 250 scientific publications in peer-reviewed journals and conferences. His research interests are antenna and sensor design, RF and microwave design circuit, metamaterials, and the IoT systems, e.g., predictive analytics, environmental monitoring, and smart cities. He is a practicing Professional Engineer of the Board of Engineers Malaysia (BEM), a National Medical Researcher (NMRR), and a Corporate Member of the Institute Engineers Malaysia (MIEM).

RAIS AHMAD SHEIKH was born in Jaunpur, India. He received the bachelor's degree in electronics & communication engineering from Ajay Kumar Garg Engineering College (AKGEC), Ghaziabad, India, in 2002, and the master's degree in digital system from the Motilal Nehru National Institute of Technology (MNNIT), Allahabad, India, in 2010. He is currently pursuing the Ph.D. degree with the School of Computer and Communication Engineering, Universiti Malaysia Perlis (UniMAP), Malaysia. After his bachelor's degree, he was a Lecturer with the Azad Institute of Engineering and Technology (AIET), Lucknow, India, from 2002 to 2008. After his master's degree, he was an Assistant Professor with Babu Banarsi Das University (BBDU), Lucknow, India, from 2010 to 2011. Since 2011, he has been a Lecturer with the Department of Electrical Engineering, Jazan University, Jazan, Saudi Arabia. His research interests include flexible antennas, wearable antennas, search and rescue antennas, characterization of materials, and extraction of permittivity.

AZREMI ABDULLAH AL-HADI (S'13–M'13–SM'14) was born in Michigan, USA. He received the M.Sc. degree in communication engineering from Birmingham University, U.K., in 2004, and the D.Sc. (Tech.) degree from Aalto University, Finland, in 2013.

He is currently an Associate Professor and the Dean of the School of Computer and Communication Engineering, Universiti Malaysia Perlis (UniMAP), where he has been with the school, since 2002. His current research interests include design and performance evaluation of multielement antennas, mobile terminal antennas and their user interactions, and wireless propagation.

Dr. Azremi is a member of the Board of Engineers Malaysia (BEM), Malaysia, and a Graduate Technologist of the Malaysia Board of Technologist (MBOT), Malaysia. He was a recipient of the Best Student Paper Award presented at the 5th Loughborough Antennas and Propagation Conference (LAPC 2009) and the CST University Publication Award, in 2011. He is the Chartered Engineer of the Institution of Engineering and Technology (IET), U.K. He is active in volunteer work with the IEEE Malaysia Section, acting as the Vice Chair of the IEEE Antenna Propagation/Microwave Theory techniques/Electromagnetic Compatibility (AP/MTT/EMC) Malaysia Chapter and a Counselor for the IEEE UniMAP Student Branch.

PRAYOOT AKKARAEKTHALIN (M'98) received the B.Eng. and M.Eng. degrees in electrical engineering from the King Mongkut's University of Technology North Bangkok (KMUTNB), Bangkok, Thailand, in 1986 and 1990, respectively, and the Ph.D. degree from the University of Delaware, Newark, DE, USA, in 1998. From 1986 to 1988, he was a Research and Development Engineer with Microtek Company Ltd., Thailand. In 1988, he joined the Department of Electrical Engineering, KMUTNB. He has authored or coauthored more than 40 international journals, more than 200 conference papers, and four books/book chapters. His current research interests include RF/microwave circuits, wideband and multiband antennas, telecommunications, and sensor systems. He is a member of the IEICE Japan, ECTI, and EEAAT Associations, Thailand. He was the Chairman of the IEEE MTT/AP/ED Thailand Joint Chapter, from 2007 to 2010, and the Vice President and President of the ECTI Association, Thailand, from 2012 to 2013 and from 2014 to 2015, respectively. He is currently the Leader of the TRF Senior Research Scholar Project of "Innovative Sensor Technology for Thailand Development" granted by the Thailand Research Fund, Thailand. He was the Editor-in-Chief for the ECTI Transactions, from 2011 to 2013.